Am J Physiol Heart Circ Physiol 283: H1634–H1644, 2002.
First published June 20, 2002; 10.1152/ajpheart.01073.2001.

Pyruvate improves redox status and decreases indicators of hepatic apoptosis during hemorrhagic shock in swine

PAUL D. MONGAN, JOHN CAPACCHIONE, SHANDA WEST, JOHN KARAIAN, DAWN DUBOIS, RYAN KENEALLY, AND PUSHPA SHARMA
Department of Anesthesiology, Uniformed Services University of the Health Sciences, Bethesda, Maryland 20814

Received 19 December 2001; accepted in final form 5 June 2002

Mongan, Paul D., John Capacchione, Shanda West, John Karaian, Dawn Dubois, Ryan Keneally, and Pushpa Sharma. Pyruvate improves redox status and decreases indicators of hepatic apoptosis during hemorrhagic shock in swine. *Am J Physiol Heart Circ Physiol* 283: H1634–H1644, 2002. First published June 20, 2002; 10.1152/ajpheart.01073.2001.—Previous studies have shown that the liver is the first organ to display signs of injury during hemorrhagic shock. We examined the mechanism by which pyruvate can prevent liver damage during hemorrhagic shock in swine anesthetized with halothane. Thirty minutes after the induction of a 240-min controlled arterial hemorrhage targeted at 40 mmHg, hypertonic sodium pyruvate (0.5 $g \cdot kg^{-1} \cdot h^{-1}$) was infused to achieve an arterial concentration of 5 mM. The volume and osmolality effects of pyruvate were matched with 10% saline (HTS) and 0.9% saline (NS). Although the peak hemorrhage volume increased significantly in both the pyruvate and HTS group, only the pyruvate treatment was effective in delaying cardiovascular decompensation. In addition, pyruvate effectively maintained the NADH/NAD redox state, as evidenced by increased microdialysate pyruvate levels and a significantly lower lactate-to-pyruvate ratio. Pyruvate also prevented the loss of intracellular antioxidants (GSH) and a reduction in the GSH-to-GSSG ratio. These beneficial effects on the redox environment decreased hepatic cellular death by apoptosis. Pyruvate significantly increased the ratio of Bcl-Xl (antiapoptotic molecule)/Bax (proapoptotic molecule), prevented the release of cytochrome *c* from mitochondria, and decreased the fragmentation of caspase 3 and poly(ADP ribose) polymerase (DNA repair enzyme). These beneficial findings indicate that pyruvate infused 30 min after the onset of severe hemorrhagic shock is effective in maintaining the redox environment, preventing the loss of the key antioxidant GSH, and decreasing early apoptosis indicators.

glutathione; redox state; caspases

DESPITE ADVANCES IN THE EARLY CARE of trauma victims over the past two decades, multiple organ failure (MOF) continues to be a major factor in the morbidity and mortality that occurs after resuscitation from hemorrhagic shock (16). While there are numerous factors that influence the development of MOF, there is increasing evidence that hepatic dysfunction plays a central role (21, 24, 42, 43). Experimental studies have shown that despite acute aggressive resuscitation, there is a consistent depression in microvascular blood flow that results in hypoperfusion and progressive hepatic dysfunction (32, 42, 43). This suggests that despite the restoration of global oxygen delivery, additional pharmacological therapies are needed to prevent or reverse ongoing hepatotoxicity. However, the precise mechanisms of hepatocellular dysfunction after severe hemorrhagic shock are not well defined. Some investigators have shown that the reduction in immunological mediators, such as tumor necrosis factor-α, improves outcome indicators (23, 41). Others have shown that there is severe hepatic energy depletion during hemorrhagic shock and that improvement in the hepatocellular energy state reduces liver dysfunction (7, 38, 40). Overall, these studies show that outcome after resuscitation is dependent on many factors.

Changes in the cellular redox environment and its ability to mediate oxidative stress during ischemia and reperfusion are major contributing factors in cellular injury and can induce cell death by either apoptosis or necrosis (11, 12, 26). While necrosis results from overwhelming cellular deenergization, recent studies suggest that the final common pathway for liver dysfunction after hemorrhagic shock is apoptosis (24). The induction of apoptosis results from transient opening of the mitochondrial permeability transition pore (MPTP) with the release of cytochrome *c*, further generation of oxidative stress, release of intracellular Ca^{2+}, and activation of a cascade of cysteine protease including caspase 3 (22, 25, 39). While numerous factors have been shown to mediate the increased open state probability of the MPTP, evidence suggest that changes in the redox state provide an early signaling mechanism for apoptosis (14, 22, 25, 39).

In this study, we sought to determine whether changes in the cellular redox environment were associated with apoptosis indicators. To test our hypothesis, we examined the ability of pyruvate to decrease the early indicators of hepatic apoptosis in a swine model

Address for reprint requests and other correspondence: P. D. Mongan, Dept. of Anesthesia, Uniformed Services Univ. of the Health Sciences, 4301 Jones Bridge Road, Bethesda, MD 20814 (E-mail: pmongan@usuhs.mil).

The costs of publication of this article were defrayed in part by the payment of page charges. The article must therefore be hereby marked "*advertisement*" in accordance with 18 U.S.C. Section 1734 solely to indicate this fact.

of severe controlled hemorrhagic shock. Pyruvate enhancement of the cellular redox environment can occur from one or more of the following mechanisms: *1*) direct neutralization of free radicals, *2*) alteration of the cytoplasmic NADH/NAD redox state, and/or *3*) enhancement of the intracellular glutathione antioxidant system. All of these could reduce opening of the MPTP and decrease apoptosis.

METHODS

After Institutional Animal Care and Use Committee approval, 24 adolescent Yorkshire swine (*Sus scrofa*) were randomized to receive either an intravenous infusion of 30% sodium pyruvate ($n = 8$), 10% NaCl ($n = 8$, osmotic control), or 0.9% NaCl ($n = 8$, volume control) 30 min after the start of controlled arterial hemorrhage. All animals were cared for according to the United States Department of Agriculture Animal Welfare Act and the National Institutes of Health *Guide for the Care and Use of Laboratory Animals*.

Animal Preparation and Monitoring

Anesthesia and hemodynamic monitoring procedures. The swine were fasted overnight with free access to water. In the morning, they were sedated with an intramuscular injection of ketamine (10 mg/kg) and anesthetized with halothane by nose cone to facilitate tracheal intubation. During surgical preparation, anesthesia was maintained with halothane (1.0–1.5% end tidal concentration) while the animals spontaneously ventilated 25% oxygen-75% nitrogen through a semiclosed circle system (Narkomed 2B, North American Drager; Telford, PA). Inspired and expired oxygen, carbon dioxide, and halothane concentrations were continuously monitored (M1026A Gas Analyzer and 68 Clinical Monitor, Hewlett-Packard; Andover, MD). The right external jugular vein was isolated, an 8.5-Fr introducer sheath was inserted, and a continuous thermodilution cardiac output pulmonary artery catheter was advanced through the sheath to measure pulmonary artery pressure and cardiac output (QVue, Abbott Critical Care; North Chicago, IL). Both femoral arteries and a femoral vein were isolated and cannulated with 8.5-Fr introducer sheaths. A micromanometer (MPC-500, Millar Instruments; Houston, TX) was inserted into the right femoral artery sheath and advanced to the midthoracic aorta for the measurement of mean arterial pressure (MAP). The second femoral artery sheath was used for controlled arterial hemorrhage, and the femoral vein was used for infusions. Physiological data were displayed on an eight-channel Hewlett-Packard model 68 clinical monitor.

Liver microdialysis. After instrumentation for physiological monitoring, a right subcostal incision was made. The animals were placed in the right lateral position, and the middle lobe of the liver was exposed. Two microdialysis probes (CMA 20, polycarbonate fiber length 10 mm; diameter 0.5 mm; 20,000-Da molecular cutoff) were inserted into the liver 2 and 3 cm caudate to the gallbladder at a distance of 3 cm from the liver edge. These probes were perfused with 0.9% NaCl at 2 μl/min using a precision, multisyringe pump (CMA 102, CMA/Microdialysis; Acton, MA). After the liver was repositioned in the abdominal cavity, the wound edges were infiltrated with bupivacaine (0.5%, 15 ml). Plastic wrap was used to restrict the intestines to the abdominal cavity, and the entire area was the area covered with plastic wrap to prevent desiccation.

Experimental Protocols

Computer-controlled arterial hemorrhage. One hour before the initiation of hemorrhage, and the expired halothane concentration was reduced to 0.8% with the animals spontaneously ventilating. Controlled arterial hemorrhage was automated to insure reproducibility. In brief, a customized computer protocol (LabView 5, National Instruments; Austin, TX) monitored the MAP and through a proportional control feedback algorithm controlled the speed and direction of a partial occlusion roller pump (MasterFlex Digital Console Drive, Cole-Parmer Instruments; Chicago, IL) that was connected to a femoral arterial cannula. At the start of the hemorrhage period, the computer program initiated blood withdrawal to decrease the MAP to 40 mmHg over 10 min. During hemorrhage, the blood was stored in a closed reservoir primed with sodium citrate (1.66 g) and porcine heparin (3,000 units) to inhibit clot formation. After the initial 10-min rapid hemorrhage, the program maintained the MAP at 40 mmHg either by withdrawal or by reinfusion of the hemorrhage blood as necessary. During the protocol, the volume of blood in the reservoir was gravimetrically measured (Sartorius LA4200, Sartorius; Edgewood, NY), and the data output was stored on computer hard disk with the time-stamped MAP. During isobaric-controlled arterial hemorrhage, the transition from compensated to decompensated hemorrhagic shock was recorded as the time when continued infusion of the hemorrhage volume (HV) was necessary to maintain the target MAP of 40 mmHg. The peak HV (PHV), which represents the maximum blood volume weighed in storage reservoir, is measured immediately before the time of decompensation. With the exception of the protocol infusions of pyruvate, 10% NaCl, or 0.9% NaCl, only the blood withdrawn to induce hypotension was administered to maintain the MAP at 40 mmHg. During the decompensatory phase of hemorrhagic shock, if all the HV was reinfused, no further therapy was used to support the MAP. Death was defined as a MAP <10 mmHg with cessation of spontaneous respiratory effort.

Pyruvate, 0.9% NaCl, and 10% NaCl infusion protocols. To determine the efficacy of pyruvate administered after the onset of hemorrhagic shock, the animals were block randomized to one of three treatment groups. *Group 1* was administered a 100 mg/kg bolus of 30% sodium pyruvate (pH 7.4) via the femoral vein, followed by 0.5 $g \cdot kg^{-1} \cdot h^{-1}$ for the duration of the protocol. In *groups 2* and *3*, a matched volume of 10% or 0.9% NaCl was bolused and infused to control for the osmolarity and volume effects of the hypertonic sodium pyruvate.

Analytic sampling procedures. Microdialysis samples were continuously collected over 30-min periods (60-μl aliquots) by an automated microfraction collector (CMA142, CMA/Microdialysis), and all analytic tests were performed within 1 h (lactate and pyruvate). One hour after insertion of the microdialysis probes, arterial blood was sampled every 30 min for measurement of pH, base excess, blood gases, and hemoglobin (IL 1610 and IL 682 CoOximeter, Instrumentation Laboratories; Lexington, KY). Heparinized blood samples for laboratory analysis were obtained every 30 min and immediately centrifuged.

Liver tissue sampling. At 0, 60, 120, and 240 min after the start of shock (H_0, H_{60}, H_{120}, and H_{240}, respectively), tissue samples were obtained from the liver for analysis. Liver tissue was taken from the edge of the left lobe and rapidly immersed in liquid isopentane at −90°C. Bleeding was controlled by application of thrombin, collagen matrix, and di-

rect pressure. After being frozen, the tissue was transferred to chilled cryovials and stored at −80°C for future analysis.

Analytic Methods

Microdialysis calibration procedures. In vitro relative recovery for each microdialysis probe was determined in triplicate before and after each experiment. The probes were immersed in a calibration standard solution at 38.5°C and perfused with 0.9% NaCl. The calibration standards were lactate (10 mM) and pyruvate (2 mM) in double-distilled deionized water. The concentrations of the nondialyzed standards were compared with the concentrations of the in vitro microdialysis samples to determine the relative recovery for each component. The relative recovery for each compound was used to estimate the in vivo extracellular concentration of the components in the immediate vicinity of the probes.

Lactate and pyruvate analysis. Lactate and pyruvate levels were measured in the plasma and microdialysate samples. These analyses were performed with a CMA 600 Analyzer (CMA/Microdialysis). This instrument performs an automated enzymatic conversion of lactate or pyruvate to H_2O_2. Peroxidase catalyses a reaction between H_2O_2 and other substrates to form the red-violet-colored quinonediimine. The rate of formation of the quinonediimine is measured at 546 nm and is proportional to the lactate and pyruvate concentrations.

Glutathione analysis. Frozen liver tissue samples were pulverized with porcelain mortars under liquid nitrogen, and GSH and GSSG were determined spectrophotometrically as previously described (36). In brief, 50 mg of frozen, pulverized tissue were homogenized with perchloric acid (1 N $HClO_4$) + 2 mM EDTA in Eppendorf tubes chilled in a Polar Block II cooling device (−20°C, Boekel Scientific; Feasterville, PA) using a Tissue Tearor (Biospec Products; Racine, WI). After centrifugation (5,000 *g*, 5 min at 0°C), the supernatant was neutralized with 2.0 M KOH and 0.3 M MOPS and centrifuged to remove the $KClO_4$ precipitate, and an aliquot assayed for GSH by the glyoxalase I reaction. *S*-lactoyl GSH formation was determined at 240 nm. For the determination of GSSG, pulverized liver was homogenized with 1 N $HClO_4$ with 2 mM EDTA and 50 mM *N*-ethyl maleimide (NEM). The NEM was added to trap the GSH and prevent its conversion to GSSG. After neutralization of the supernatant and removal of $KClO_4$, NEM was removed by anion exchange chromatography (QAE Sephadex). The GSSG eluent was concentrated with an evaporator, and its amount was determined spectrophotometrically at 340 nm.

NADPH and NADP analysis. NADP and NADPH were determined by reverse-phase HPLC analysis as previously described (4). In brief, to insure optimal recovery, NADP content was determined after acid extraction and NADPH was determined after alkaline extraction from frozen pulverized liver tissue. Extracts were equilibrated to a pH between 6 and 7, and 25 μl were automatically injected into a heated (35°C) Waters Symmetry Shield RP-18 column (4.6 × 150) by a refrigerated (4°C) autosampler (Waters 2690 Separations Module, Waters Associates; Milford, MA). The injectate was eluted with a 0.1 M KH_2PO_4-acetonitrile (2.5–25% vol/vol) buffer gradient. The chromatograms and absorbance data from the photodiode array (Water 996, Waters Associates) were recorded and analyzed using the Millenium 32 software (Waters Associates). Peak identification and quantification were accomplished by matching the spectral signal of the peaks, peak purity, and peak areas to the spectral signal and peak areas generated for the injected standards.

Assessment of Apoptosis [Bcl-Xl, Bax, Cytochrome c, Caspase 3, and Poly(ADP-Ribose) Polymerase Fragmentation]

Tissue preparation. Cell death by apoptosis was examined by Western immunoblotting in cell lysates or cytosolic preparations from liver tissue. In brief, pulverized frozen samples of liver tissue were lysed in 1:10 (wt/vol) ice-cold lysis buffer consisting of 25 mg/ml PBS, 230 mg/ml PMSF, 1 μg/ml leupeptin, and 1 μg/ml aprotinin in 1% Triton X-100. After brief sonication, samples were centrifuged at 1,000 *g*. The pellet S10 or cell lysate was used for the immunostaining with caspase 3 and poly(ADP-ribose) polymerase (PARP) antibodies. Liver cytosol was prepared by spinning the cell lysate at 100,000 *g* in a Beckman ultracentrifuge (TL-100). The supernatant S100 or cytosol was removed and used for immunostaining with Bcl-Xl, Bax, and cytochrome *c* antibodies.

Detection of Bcl-Xl, Bax, and cytochrome c. Cytosolic protein (25 μg) was lysed in sample buffer [62.5 mmol Tris·HCl (pH 6.8), 2% SDS, 10% glycerol, 5% β-mercaptoethanol, and 0.005% bromophenol blue] and subjected to SDS-polyacrylamide gel electrophoresis using minigel equipment (Bio-Rad). Ten percent polyacrylamide gels were used for analysis of Bcl-Xl and Bax expression, and 14% gels were used for cytochrome *c*. After electrophoresis, proteins were transferred to nitrocellulose membranes using miniblot equipment. Nonspecific proteins were blocked in 5% nonfat dried milk in Tris-buffered saline (TBS) containing 0.05% Tween 20 (TBS-T). Primary antibodies were diluted in blocking buffer and incubated with the blots for 1 h. Bcl-Xl, Bax, and cytochrome *c* (mouse monoclonal antibody at 1:500) were used. Blots were washed thoroughly with TBS-T and incubated in secondary antibody (peroxidase-conjugated goat anti-mouse, diluted 1:2,000 in blocking buffer) for 1 h. After a final wash in TBS-T, horseradish peroxidase was detected using ECL reagent (Amersham).

Caspase 3 and PARP fragmentation. Cell lysates from the liver were denatured in Laemmli sample buffer with 6 M urea for PARP and no urea for caspase 3. HL 60 cell extracts treated with etoposide to undergo apoptosis (BioMol; Plymouth Meeting, PA) were used as positive controls for the presence of the 85-kDa fragment of PARP. Proteins were resolved on 10% SDS gel and transferred to nitrocellulose membranes. For detection of caspase 3, the membrane was incubated with primary mouse monoclonal antibody from Oncogene (Gaithersburg, MD). Intact and fragmented PARP was detected by probing the membrane with primary mouse monoclonal antibody (1:2,000, BioMol), which detects both intact PARP (116 kDa) and the apoptosis-associated fragment (85 kDa). The membranes were then incubated with secondary antibody directed toward goat anti-mouse IgG (1:2,000). Negative controls were performed by omitting primary antibody as well as probing with actin. Chemiluminescence was detected by autoradiography, and the integrated optical density (OD) of the protein bands was measured using the Scion Image program.

Data Presentation and Statistics

All data are presented as means ± SE. To avoid spurious results due to multiple testing, differences within groups over the course of the experiment were determined by repeated-measures ANOVA. Differences between groups for nonrecurring measurements were assessed using ANOVA. Differences between groups over the course of the experiment were determined using a two-way ANOVA for one factor (dependent variable) over time. Within- and between-group testing

was accompanied by a Tukey's honestly significant difference multiple-range test to correct for the multiple comparisons. Proportions were evaluated using McNemar's test of proportions. Values were considered statistically different when $P < 0.05$ after correction for multiple comparisons. Error bars in the figures represent SE.

RESULTS

The animal weights were similar in the pyruvate and 10% and 0.9% NaCl groups (31.8 ± 0.9, 32.4 ± 1.1, and 31.1 ± 1.3 kg, respectively). Thirty minutes after the start of controlled arterial hemorrhage, the bolus and infusion of pyruvate raised the arterial pyruvate concentration from 0.09 ± 0.01 mM at H_{30} to 4.43 ± 0.63 mM at H_{60}. In the 10% and 0.9% NaCl groups, the pyruvate levels at H_{30} were 0.11 ± 0.02 and 0.13 ± 0.2 mM and increased to only 0.39 ± 0.03 and 0.45 ± 0.06 mM, respectively, during hemorrhage.

Hemodynamic and Hemorrhage-Related Parameters

MAP was similar in all groups before the start of the controlled arterial hemorrhage (99.6 ± 2.7, 100.5 ± 3.4, and 101.7 ± 1.0 mmHg) in the pyruvate, 10%, and 0.9% NaCl groups. Because of the automation of the hemorrhage protocol, there were no differences between the groups in the time to reach the target MAP of 40 mmHg or the variability in the MAP. However, there was a significant difference in the PHV in the pyruvate and 10% NaCl treatment groups (45.8 ± 1.2 and 42.3 ± 0.6 ml/kg) compared with the 0.9% NaCl group (34.8 ± 0.9 ml/kg, $P < 0.05$). Although there was a significant increase in the PHV in both the pyruvate and 10% NaCl groups, only the pyruvate treatment was effective in delaying cardiovascular decompensation as evidenced by the increased time to PHV (94 ± 5 vs. 73 ± 6 and 70 ± 4 min, $P < 0.05$). In addition to the delay in the decompensatory phase of hemorrhagic shock in the pyruvate group, there were significant differences in the cardiovascular profiles during the last 2 h of the hemorrhage that affected the rate of hemorrhage volume reinfusion. As detailed in Table 1, at H_{180}, both the 10% and 0.9% NaCl groups had a decrease in heart rate (HR) and were unable to increase the cardiac index despite the reinfusion of a larger amount of the HV. This decrement in cardiovascular function resulted in complete reinfusion of the HV in four animals in the both the 10% and 0.9% NaCl groups, progressive decreases in the MAP, and death. This profile indicates significantly compromised cardiovascular function. In contrast, despite the smaller amount of HV return, the pyruvate-treated animals had no decreases in HR, had greater augmentation of the cardiac index, and suffered only one animal death throughout the protocol. Thus the pyruvate treatment

Table 1. *Hemorrhage volume and physiological measurements*

	Time								
	H_0	H_{30}	H_{60}	H_{90}	H_{120}	H_{150}	H_{180}	H_{210}	H_{240}
n									
Pyruvate	8	8	8	8	8	8	8	8	7
10% NaCl	8	8	8	8	8	7	6	4	4
0.9% NaCl	8	8	8	8	8	7	6	6	4
HV, ml/kg									
Pyruvate	0	26.6 ± 1.7	41.2 ± 1.8	43.6 ± 1.6	42.3 ± 1.8	34.6 ± 1.7	29.1 ± 2.1	22.6 ± 1.9	18.5 ± 2.9
10% NaCl	0	25.9 ± 1.1	39.5 ± 1.4	38.5 ± 1.8	35.3 ± 1.7*	25.1 ± 1.8*	17.2 ± 2.4*	9.4 ± 2.3*	7.9 ± 4.2
0.9% NaCl	0	26.3 ± 1.2	33.5 ± 1.3*	31.8 ± 0.9*	27.1 ± 1.2*	20.6 ± 2.0*	16.1 ± 2.8*	10.2 ± 2.6*	8.2 ± 3.1
HR, beats/min									
Pyruvate	125 ± 9	212 ± 10	253 ± 9	252 ± 7	248 ± 8	251 ± 8	246 ± 6	245 ± 9	242 ± 8
10% NaCl	133 ± 11	204 ± 8	247 ± 12	249 ± 8	246 ± 7	234 ± 12	217 ± 10*	205 ± 7*	197 ± 11*
0.9% NaCl	135 ± 8	208 ± 11	250 ± 7	251 ± 6	245 ± 9	229 ± 10	212 ± 11*	209 ± 11*	190 ± 12*
MAP, mmHg									
Pyruvate	99.6 ± 2.7	40.4 ± 0.1	40.2 ± 0.1	40.0 ± 0.1	39.9 ± 0.3	39.7 ± 0.3	39.4 ± 0.3	39.4 ± 9	39.1 ± 1.2
10% NaCl	100.5 ± 3.4	40.3 ± 0.2	39.9 ± 0.1	39.4 ± 0.8	39.2 ± 0.2	39.4 ± 0.3	38.2 ± 0.7	38.5 ± 1.7	27.1 ± 4.9*
0.9% NaCl	101.7 ± 1.0	40.3 ± 0.2	40.1 ± 0.1	39.9 ± 0.1	38.7 ± 0.5	39.8 ± 0.2	38.8 ± 0.2	38.6 ± 0.7	32.4 ± 2.9
CVP, mmHg									
Pyruvate	1.4 ± 1.0	−5.7 ± 0.9	−6.2 ± 1.1	−6.7 ± 1.1	−6.5 ± 1.0	−5.6 ± 0.9	−5.3 ± 0.8	−5.2 ± 0.9	−4.9 ± 0.9
10% NaCl	1.1 ± 0.9	−5.5 ± 1.1	−6.1 ± 0.9	−6.4 ± 0.9	−5.7 ± 1.1	−5.0 ± 1.2	−4.1 ± 1.2	−4.1 ± 1.1	−3.8 ± 1.2
0.9% NaCl	1.4 ± 0.7	−5.9 ± 0.7	−6.1 ± 1.0	−6.2 ± 0.9	−5.8 ± 1.2	−5.1 ± 1.1	−4.7 ± 1.0	−3.8 ± 0.9	−3.5 ± 0.9
CI, $ml \cdot kg^{-1} \cdot min^{-1}$									
Pyruvate	178.2 ± 12.8	66.3 ± 4.2	48.4 ± 4.2	41.5 ± 3.6	45.0 ± 2.7	54.6 ± 3.3	61.2 ± 3.6	69.5 ± 5.1	70.8 ± 4.7
10% NaCl	174.5 ± 15.6	61.6 ± 4.7	49.1 ± 4.7	37.8 ± 3.4	39.2 ± 2.9	44.9 ± 4.3	45.8 ± 3.7*	44.6 ± 4.5*	46.2 ± 5.1*
0.9% NaCl	184.8 ± 8.1	67.3 ± 3.5	50.3 ± 4.4	35.5 ± 3.3	38.1 ± 2.4	42.4 ± 4.1	46.6 ± 5.6*	43.3 ± 5.8*	39.5 ± 1.3*
SV, ml/beat									
Pyruvate	45.2 ± 2.8	11.4 ± 1.6	6.2 ± 0.9	4.7 ± 0.5	5.5 ± 0.5	6.4 ± 0.4	7.8 ± 0.6	8.4 ± 0.8	9.1 ± 1.0
10% NaCl	44.9 ± 3.2	11.8 ± 1.7	6.6 ± 0.8	4.6 ± 0.8	5.1 ± 0.5	6.1 ± 0.7	6.9 ± 0.5	7.6 ± 0.9	8.3 ± 0.7
0.9% NaCl	47.1 ± 3.1	12.3 ± 1.5	6.9 ± 0.6	4.8 ± 0.4	5.6 ± 0.5	6.2 ± 0.6	7.4 ± 0.7	8.4 ± 0.9	8.6 ± 0.9

Data are presented as means ± SE; *n* = no. of swine. The initial hemodynamic measurements were made immediately before the start of the controlled arterial hemorrhage. Subscripted numbers refer to minutes. The pyruvate, 10% NaCl (osmotic control), or 0.9% NaCl (volume control) treatments were started 30 min after the start of hemorrhage (H_{30}). HV, hemorrhage volume; HR, heart rate; MAP, mean arterial pressure; CVP, central venous pressure; CI, cardiac index; SV, stroke volume. *$P < 0.05$ compared with the pyruvate group for the time-matched data.

delayed the onset of the decompensatory stage of hemorrhagic shock by increasing the time to PHV. In addition, during decompensation, the pyruvate-treated animals had a greater tolerance to the prolonged hypotension during hemorrhagic shock, as indicated by a more favorable cardiac function than the 10% and 0.9% NaCl groups.

Osmolality and Acid Base Parameters

Table 2 shows that there were significant increases and decreases in osmolality and hemoglobin, respectively, in the pyruvate and 10% NaCl groups. The changes were similar in those groups and significantly different compared with the 0.9% NaCl group. This indicates that the delay in cardiovascular decompensation in the pyruvate group was not related to either the volume or osmotic effects of the treatment. After the first 30 min of hemorrhage, all groups had *1*) similar increases in lactate and the lactate-to-pyruvate ratio and *2*) decreases in base excess (Table 2). However, after the initiation of the pyruvate or NaCl treatments, there were significant differences between the groups for the remainder of the protocol. After H_{30} in the NaCl groups, there were continued significant increases in lactate and the lactate-to-pyruvate ratio and decreases in base excess and pH. In comparison, although the pyruvate treatment caused lactate to increase two times higher than the other groups, the lactate-to-pyruvate ratio, the more relevant indicator of metabolic stress, decreased to one-half the initial value. In addition, the pyruvate administration prevented the magnitude of changes in acid-base parameters that occurred in the other groups.

Pyruvate Effects on Liver Microdialysis Lactate-to-Pyruvate Ratio

Figure 1 illustrates the differences between the treatment groups and the microdialysate lactate-to-pyruvate ratio measurements. The lactate, pyruvate, and lactate-to-pyruvate ratio was similar in both groups before (H_0) and 30 min after the start of hemorrhage (H_{30}; before treatment). However, the pyruvate infusion increased the microdialysate pyruvate levels from 0.07 to 1.62 mM during the experiment compared with the increases to 0.15 and 0.13 mM in the 10% and 0.9% NaCl animals, respectively ($P < 0.05$). Compared with the NaCl control groups, this rise in pyruvate resulted in a significantly lower and stable lactate-to-pyruvate ratio until the end of the protocol (H_{240}).

Pyruvate Effects on GSH/GSSG and NADP/NADPH

Figure 2 depicts the results of the GSH/GSSG levels and ratios in the groups during hemorrhagic shock. Basal levels of GSH and GSSG were similar in

Table 2. *Osmolality, hemoglobin, lactate, and acid-base status*

	Time								
	H_0	H_{30}	H_{60}	H_{90}	H_{120}	H_{150}	H_{180}	H_{210}	H_{240}
n									
Pyruvate	8	8	8	8	8	8	8	8	7
10% NaCl	8	8	8	8	8	7	6	4	4
0.9% NaCl	8	8	8	8	8	7	6	6	4
Osmolality, meq/l									
Pyruvate	271 ± 3	270 ± 3	297 ± 5	308 ± 4	311 ± 5	316 ± 5	318 ± 4	320 ± 4	325 ± 5
10% NaCl	269 ± 3	269 ± 2	299 ± 5	309 ± 4	309 ± 4	319 ± 5	320 ± 5	324 ± 6	327 ± 6
0.9% NaCl	268 ± 3	266 ± 3	266 ± 3*	267 ± 2*	267 ± 3*	268 ± 3*	270 ± 3*	270 ± 3*	269 ± 5*
Hemoglobin, g/dl									
Pyruvate	9.6 ± 0.1	8.7 ± 0.2	7.5 ± 0.2	6.7 ± 0.2	6.9 ± 0.3	7.0 ± 0.3	7.1 ± 0.3	7.1 ± 0.3	7.1 ± 0.3
10% NaCl	9.9 ± 0.1	8.9 ± 0.2	7.4 ± 0.2	6.6 ± 0.2	6.9 ± 0.3	7.0 ± 0.3	7.0 ± 0.3	7.2 ± 0.4	7.4 ± 0.5
0.9% NaCl	9.7 ± 0.1	8.6 ± 0.2	8.7 ± 0.3*†	9.0 ± 0.4*†	9.7 ± 0.5*†	9.9 ± 0.4*†	9.8 ± 0.4*†	9.8 ± 0.3*†	9.9 ± 0.4*†
Lactate, mM									
Pyruvate	1.2 ± 0.2	3.1 ± 0.2	12.3 ± 1.6	19.6 ± 0.9	26.4 ± 1.1	27.9 ± 0.8	28.2 ± 1.0	29.6 ± 1.1	30.9 ± 1.5
10% NaCl	1.2 ± 0.1	3.2 ± 0.2	6.6 ± 1.4*	11.4 ± 1.1*	12.5 ± 1.0*	13.2 ± 1.0*	14.1 ± 0.6*	14.7 ± 0.7*	13.2 ± 1.1*
0.9% NaCl	1.1 ± 0.1	3.3 ± 0.3	7.0 ± 1.3*	10.8 ± 0.8*	11.5 ± 0.6*	11.9 ± 0.5*	13.3 ± 0.4*	14.2 ± 0.6*	12.0 ± 1.0*
Lactate/pyruvate									
Pyruvate	14.2 ± 1.3	25.9 ± 4.2	4.7 ± 0.5	4.4 ± 0.4	4.8 ± 0.4	5.1 ± 0.6	5.2 ± 0.5	5.8 ± 0.6	6.0 ± 0.7
10% NaCl	13.6 ± 1.6	26.6 ± 4.4	34.8 ± 3.7*	36.9 ± 3.8*	37.2 ± 3.6*	39.7 ± 3.1*	37.3 ± 2.3*	35.4 ± 2.1*	36.2 ± 2.5*
0.9% NaCl	13.5 ± 1.4	24.6 ± 3.7	31.5 ± 2.1*	33.2 ± 2.4*	34.7 ± 3.3*	33.1 ± 2.7*	33.0 ± 2.6*	34.2 ± 1.4*	33.2 ± 1.5*
Base excess, meq/l									
Pyruvate	4.4 ± 0.6	−1.4 ± 0.4	−1.8 ± 1.0	−2.1 ± 1.6	−1.7 ± 1.4	−1.5 ± 1.9	0.7 ± 2.1	4.7 ± 2.6	5.1 ± 2.2
10% NaCl	4.8 ± 0.8	−1.1 ± 0.9	−5.9 ± 1.5	−11.4 ± 2.1*	−13.7 ± 2.0*	−17.7 ± 1.2*	−17.0 ± 1.0*	−17.3 ± 1.5*	−16.4 ± 2.7*
0.9% NaCl	4.4 ± 0.6	−0.9 ± 0.5	−5.4 ± 1.1	−10.1 ± 1.3*	−11.9 ± 1.0*	−13.6 ± 1.2*	−14.5 ± 1.2*	−14.4 ± 1.5*	−14.9 ± 2.1*
pH									
Pyruvate	7.41 ± 0.01	7.38 ± 0.02	7.37 ± 0.04	7.38 ± 0.06	7.39 ± 0.04	7.38 ± 0.05	7.39 ± 0.06	7.41 ± 0.03	7.42 ± 0.05
10% NaCl	7.43 ± 0.01	7.40 ± 0.02	7.35 ± 0.03	7.25 ± 0.04	7.18 ± 0.05*	7.14 ± 0.04*	7.10 ± 0.05*	7.14 ± 0.07*	7.14 ± 0.08*
0.9% NaCl	7.42 ± 0.01	7.41 ± 0.02	7.36 ± 0.02	7.26 ± 0.03	7.24 ± 0.06*	7.20 ± 0.04*	7.17 ± 0.04*	7.16 ± 0.06*	7.17 ± 0.05*

Data are presented as means ± SE; *n* = no. of swine. The initial measurements were made immediately before the start of the controlled arterial hemorrhage. The pyruvate, 10% NaCl, or 0.9% NaCl treatments were started 30 min after the start of hemorrhage (H_{30}). *$P < 0.05$ compared with the pyruvate group for the time-matched data; †$P < 0.05$ compared with the 10% NaCl group for the time-matched data.

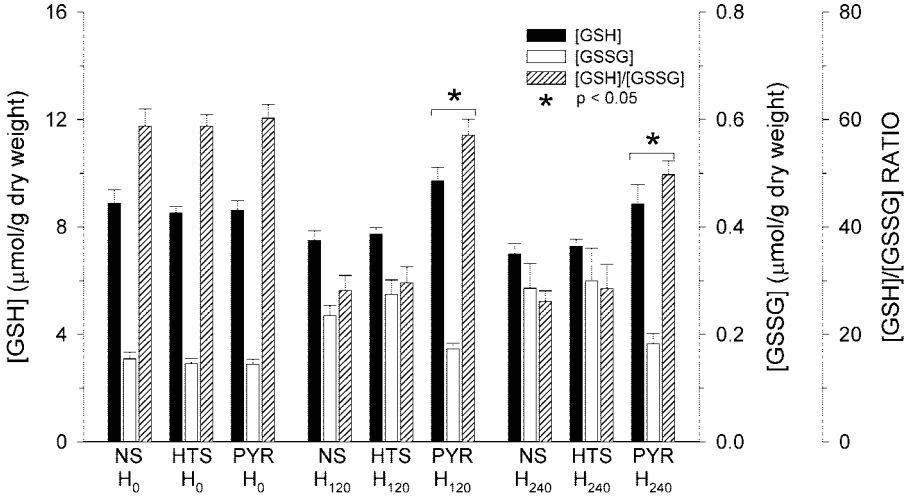

Fig. 1. Beneficial effects of pyruvate administration on GSH and diminution of the GSH-to-GSSG ratio (GSH/GSSG) during controlled arterial hemorrhage. At both 120 and 240 min after the start of shock (H_{120} and H_{240}), the pyruvate-treated animals had significantly higher GSH content and GSH/GSSG compared with the 10% NaCl (HTS) and 0.9% NaCl (NS)-treated animals.

all groups. Compared with the 10% and 0.9% NaCl animals, pyruvate maintained significantly higher levels of the intracellular antioxidant GSH at both H_{120} and H_{240}. Subsequently, the GSH-to-GSSG ratio in the pyruvate group was only slightly reduced at H_{240}, whereas there was a loss of total glutathione and a 50–60% reduction in GSH-to-GSSG ratio at both H_{120} and H_{240} in the other groups. Evaluation of NADP and NADPH levels showed that NADPH was similar at baseline in all the pyruvate and 10% and 0.9% NaCl animals (0.31 ± 0.01, 0.32 ± 0.02, and 0.32 ± 0.01 μM/g dry wt). Whereas the NADPH levels decreased similarly at H_{240} in the 10% and 0.9% NaCl animals (0.24 ± 0.02 and 0.26 ± 0.02 μM/g dry wt), the NADPH levels in the pyruvate animals were increased to 0.41 ± 0.03 μM/g dry wt at H_{240} and the NADPH-to-NADP ratio was increased by 1.5–2 times during the infusion of pyruvate. These findings are important because regeneration of GSH is carried out by the enzyme glutathione reductase, which requires the cofactor NADPH.

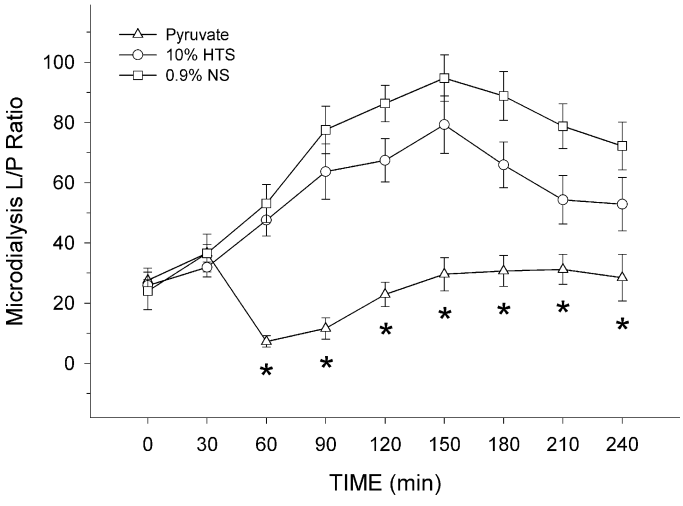

Fig. 2. Changes in the microdialysis lactate-to-pyruvate ratio (L/P) during the protocol. The increase in the 10% and 0.9% NaCl animals were due to a rapid and significant increase in lactate.

Pyruvate Effects on Apoptosis-Related Parameters

As shown in Table 3, the OD of Bcl-Xl in the pyruvate-treated group was significantly higher than that in the 10% NaCl or 0.9% NaCl groups ($P < 0.05$, $n = 8$). On the other hand, Bax expression was slightly lower in the pyruvate-treated group ($P > 0.05$). To further characterize the balance between Bcl-Xl and Bax in liver tissue, the Bcl-Xl-to-Bax ratio was calculated using the mean OD in autoradiographs after immunoblotting. At H_{240}, the pyruvate-treated animals had a significant higher ratio of Bcl-Xl to Bax compared with the 10% and 0.9% NaCl animals (1.63 vs. 0.35 and 0.59, respectively, $P < 0.05$). Representative examples are presented in Fig. 3. This difference is significant because the Bcl-Xl-to-Bax ratio is a significant factor in the induction of apoptosis by preventing mitochondrial depolarization and blocking the release of cytochrome *c*. Thus it represents the functional relevant checkpoint for the regulation of apoptosis. This increased Bcl-Xl-to-Bax ratio is consistent with the absence of cytochrome *c* detection in the pyruvate-treated animals compared with the consistent detection in all the 10% and 0.9% NaCl animals.

Table 3. *Differential expression of Bcl-Xl and Bax in treatment groups*

Treatment	Bcl-Xl	Bax	Bcl-Xl
Pyruvate	1.53 ± 0.22*	0.94 ± 0.17	1.63*
0.9% NaCl	0.77 ± 0.11	1.29 ± 0.19	0.59
10% NaCl	0.47 ± 0.06	1.36 ± 0.21	0.35

Numbers indicate means ± SE of optical density (OD) from each treatment group, which consisted of 8 animals. Expression of Bcl-Xl and Bax was measured in liver tissue obtained at 240 min after the start of controlled arterial hemorrhagic shock in animals treated with pyruvate, 0.9% NaCl, or 10% NaCl. Cellular cytosolic preparations from liver tissue were subjected to SDS-PAGE, and Western blot was performed using the monoclonal anti-Bcl-Xl or anti-BAX and a peroxidase-conjugated secondary antibody. In negative controls, primary antibodies were omitted. Ponceau staining in membranes indicated an equal amount of protein loaded per lane (data not shown). *$P < 0.05$ compared with the other groups.

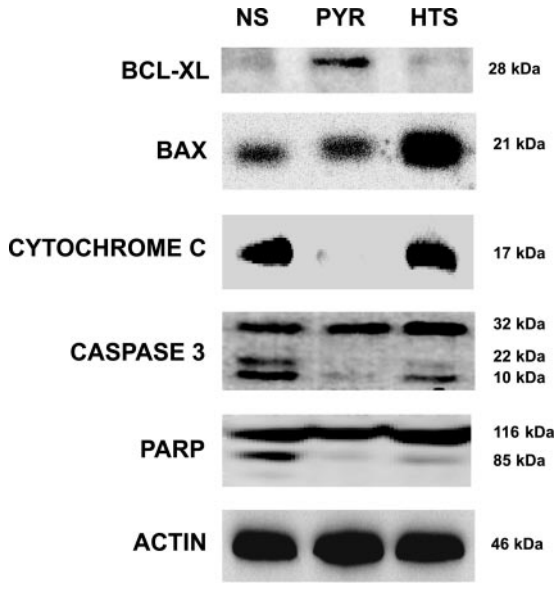

Fig. 3. Representative Western blots of the effects of pyruvate administration on critical indicators of hepatic apoptosis. Liver samples were obtained 240 min after the start of hemorrhagic shock or after complete infusion of the shed blood volume if/when complete cardiac collapse was imminent. The immunoblots demonstrate the increase in Bcl-Xl with similar Bax bands. Cytochrome *c* was not detectible in the pyruvate sample. Finally, there was increased activation of caspase 3 and poly(ADP-ribose) polymerase (PARP) fragmentation in the 10% and 0.9% NaCl animals.

Further evidence for the beneficial effect of pyruvate in decreasing apoptosis indicators during the prolonged period of hemorrhagic shock is presented in Table 4 and Fig. 3. As shown in the representative immunoblot in Fig. 3, cytochrome *c* was detected in the cytosolic fractions of the 10% and 0.9% NaCl groups and not in the pyruvate-treated animals. The activation of caspase 3 in cell extracts from liver samples in 10% and 0.9% NaCl groups is indicated by the increased detection of caspase 3 subunits. The 32-kDa proenzyme of caspase 3 is cleaved at specific aspartate residues to generate two smaller active subunits (21 and 10 kDa), which oligomerize to form an active protease complex. At H_{240}, the OD of 32-kDa protein was 0.81 ± 0.03, 0.64 ± 0.1, and 0.43 ± 0.02 in the pyruvate, 10% NaCl, and 0.9% NaCl animals. The OD of the active subunit of 21 kDa was 0.02 ± 0.01, 0.54 ± 0.1, and 0.41 ± 0.11 in the pyruvate, 10% NaCl, and 0.9% NaCl animals. This data represents only 3% activation of caspase 3 in the pyruvate group compared with 40% and 56% of the total caspase 3 in the 10% and 0.9% NaCl groups. These findings are not surprising because the release of cytochrome *c* is involved in the execution phase of apoptotic cell death via cytoplasmic proteolytic cascades that lead to caspase 3 activation. Another important process involved in apoptosis is the cleavage of PARP. At H_{240}, liver tissue from 10% and 0.9% NaCl animals exhibited significantly lower amounts of intact PARP (116 kDa, 2.63 ± 0.16 and 2.94 ± 0.33, $n = 8$) compared with the pyruvate-treated group (3.27 ± 0.27, $n = 8$, $P < 0.05$). The OD of fragmented PARP (85 kDa) was 1.5%, 26%, and 28% of the total PARP in the pyruvate, 10% NaCl, and 0.9% NaCl groups, respectively.

DISCUSSION

The present study indicates that infusion of pyruvate (5 mM) 30 min after the onset of severe controlled hemorrhagic shock suggests that pyruvate attenuated the initiation and execution phase of apoptotic cell death. This is indicated by the decreased release of cytochrome *c* from the mitochondria and reduced fragmentation of caspase 3 and PARP in the pyruvate liver samples obtained after the 4-h period of hypotension. This beneficial effect of pyruvate could be secondary to *1*) the alteration in the cytosolic redox state, as indicated by the microdialysate lactate-to-pyruvate ratio; *2*) the maintenance of a stable hepatic redox environment, as indicated by the GSH-to-GSSG ratio; *3*) maintenance of total glutathione content by the prevention of GSH efflux; and/or *4*) by limiting the hypotension induced changes in acid-base parameters.

We have previously shown that pyruvate treatment during controlled arterial hemorrhage prevents cardiovascular decompensation, delays the onset of the decompensatory phase of hemorrhagic shock, and significantly prolongs survival (29, 30). In this study, although there was no difference in the PHV between the pyruvate and 10% NaCl treatments, we again observed a delay in the onset of the decompensatory phase of shock as indicated by the longer time before the start of the HV to maintain the MAP in the pyru-

Table 4. *Caspase 3 and PARP immunoblot signal intensity*

Protein	Pyruvate	0.9% NaCl	10% NaCl
Intact caspase 3 (32 kDa)	0.81 ± 0.03*	0.43 ± 0.02	0.64 ± 0.16
Activated caspase 3 (21 kDa)	0.02 ± 0.01*	0.54 ± 0.10	0.41 ± 0.11
Total caspase 3 (32 + 21 kDa)	0.83 ± 0.17	0.97 ± 0.21	1.05 ± 0.62
%Activated caspase 3 [(21/32 kDa)100]	3%*	56%	40%
Intact PARP (116 kDa)	3.27 ± 0.27	2.94 ± 0.33	2.63 ± 0.16
Fragmented PARP (85 kDa)	0.05 ± 0.03*	1.15 ± 0.08	0.93 ± 0.05
Total PARP (116 + 85 kDa)	3.32 ± 0.63	4.09 ± 0.92	3.56 ± 0.41
%PARP fragmentation [(85 kDa/116)100]	1.5%*	28%	26%

Number indicate mean ± SE of OD from each treatment group, which consisted of 8 animals. Activation of caspase 3 and fragmentation of poly(ADP-ribose) polymerase (PARP) was measured in liver tissue obtained at 240 min after the start of controlled arterial hemorrhagic shock in animals treated with pyruvate, 0.9% NaCl, or 10% NaCl. Whole cell lysates from liver tissue were subjected to SDS-PAGE, and Western blot was performed using the monoclonal anti-caspase 3 or anti-PARP and a peroxidase-conjugated secondary antibody. In negative controls, primary antibodies were omitted. Ponceau staining in membranes indicated an equal amount of protein loaded per lane (data not shown). *$P < 0.05$ compared with the other groups.

vate group. While there are several metabolic and cardiovascular mechanisms that may be responsible for this observation, this salutary effect cannot be attributed to differences in volume status because of the similar changes in osmolality and hemoglobin in these two groups during the protocol.

In addition to the delay in the decompensatory phase of hemorrhagic shock, pyruvate administration during controlled arterial hemorrhagic shock improved key measures of cellular redox environment, antioxidant reserve, and indicators of cellular apoptosis. Cells die via two pathways: necrosis or apoptosis (programmed cell death). Necrosis is a form of cell death that is caused by physical, chemical, or osmotic damage with consecutive disruption of internal and external membranes, leading to cell swelling and lysis with release of cytoplasmic material. In contrast, apoptosis is an innate cellular program of cell death. Apoptosis is regulated by energy-dependent mechanisms that involve a cascade of biochemical events resulting in cell shrinkage, chromatin condensation, DNA fragmentation, and ultimately cell death. While there are significant differences in these two types of cell death, during ischemia they are a continuum of damage that occurs secondary to the duration of the increase in the open state of the MPTP (1, 14, 17, 22). While the open state probability of the MPTP increases with higher concentrations of Ca^{2+} in the mitochondria, the sensitivity can be increased by changes in the redox state, oxidative stress, and adenine nucleotide depletion (15). During apoptosis, opening of the MPTP is insufficient to result in complete mitochondrial failure. However, it is sufficient to cause mitochondrial swelling and cytochrome *c* release. The release of cytochrome *c* subsequently activates the apoptotic cascade and eventually causes cell death.

Whereas pyruvate has been documented to have beneficial myocardial functional effects secondary to metabolic alterations, Kerr et al. (19) has shown that the ability of pyruvate to decrease the open state probability of the MPTP during ischemia-reperfusion is unrelated to its metabolic enhancing effects. During ischemia, two redox-sensitive mechanisms have been implicated in the increased open state probability of the MPTP. The first is sensitive to decreases in GSH and the second is sensitive to an increase in the NADH-to-NAD ratio.

Glutathione is the major thiol-disulfide redox buffer of the cell. The redox pair GSH/GSSG provides a large pool of reducing equivalents and is thus not only an indicator of the redox state of the cell but the redox environment/buffering capacity of the cell as well. If there is insufficient NADPH to regenerate GSH, there is an overall shift in the redox state to a more positive potential. If this shift is not corrected by the regeneration of GSH, GSSG is exported to compensate for the deleterious shift in the redox state (34). Thus efflux of glutathione from the cell with subsequent loss of total content is an indicator of oxidative stress.

In previous evaluations, pyruvate has been observed to decrease apoptosis during oxidant stress (5, 19). One of the potential mechanisms for the decrease in apoptosis markers in this study is the ability of pyruvate to favorably alter these indicators of the cytosolic redox environment. Pyruvate administration has been shown to improve the NADH-to-NAD ratio and GSH-to-GSSG ratio, the key endogenous defense mechanism against oxidative stress (18, 36). Whereas the changes in the NADH-to-NAD ratio are affected through the conversion of pyruvate to lactate, the effect on GSH-to-GSSG ratio occurs when citric acid intermediates are increased through mitochondrial carboxylation of pyruvate. The elevated citrate concentration inhibits phosphofructokinase and diverts glycolytic flux into the hexose monophosphate shunt, the principal source of cytosolic NADPH (36). GSH is regenerated from oxidized glutathione disulfide, GSSG is generated by glutathione reductase, and NADPH is the source of the reducing equivalents for this reaction. In this current study, pyruvate administration increased the NADPH-to-NADP ratio, maintained the GSH-to-GSSG ratio, and prevented decreases in the GSH pool. While these findings have been observed in endothelial cell culture and isolated heart preparations, this is the first study to link these changes in the cytosolic redox environment and a decrease in apoptosis markers. From the data presented, it is apparent that the administration of pyruvate during hemorrhagic shock had several beneficial effects on cellular function and reduced multiple measures of apoptosis. One beneficial effect of pyruvate in preventing the apoptosis is the favorable maintenance of the hepatic GSH-to-GSSG ratio and prevention of a decrease in total glutathione content throughout the study. Other studies performed during hemorrhagic shock and hypoxia have shown that the hepatic GSH-to-GSSG ratio is reduced and there is an efflux of glutathione content from the liver (20). This was prevented by the administration of pyruvate in the current study. In addition, other studies have shown a temporal link between decreases in GSH and the GSH-to-GSSG ratio and activation of caspase 3 and PARP fragmentation (44). Isolated rat hepatocytes with moderate depletion of GSH results in apoptosis, and cardiomyocyte apoptosis has been shown to be regulated by redox-sensitive transcription factors (27, 31). These studies in concert with our data support the concept that deleterious alterations in the cytosolic thiol redox state results in activation of factors leading to apoptosis.

In addition to improving the thiol redox state of the hepatic tissue, pyruvate administration also improved the microdialysis lactate-to-pyruvate ratio, an indicator of the NADH/NAD cytosolic redox state. The marked increase in the lactate-to-pyruvate ratio in the 0.9% and 10% NaCl swine is an indicator of an increase in NADH and the cytosolic NADH-to-NAD ratio. When considering the redox pairs NADPH/NADP and NADH/NAD, pyruvate causes distinctly opposite but beneficial effects. NADPH is a reductive cofactor that serves as an electron donor in the regeneration of GSH. However, in the cytosol, pyruvate administration decreases the NADH-to-NAD ratio via

the conversion of pyruvate to lactate. In this instance, NAD serves as a sink for electrons and functions to reduce oxidative stress (34). Both of these changes help to maintain a favorable reduction of the cytosol, thus decreasing oxidative signaling for an increased open state probability of the MPTP. As opposed to the increase in lactate and NADH during hemorrhagic shock, the decrease in the lactate-to-pyruvate ratio by pyruvate indicates a favorable change in the NADH-to-NAD ratio with a reduction in the redox potential. Compared with the beneficial effects of pyruvate, increases in the NADH-to-NAD ratio in hepatocytes through the use of NADH-generating substrates (ethanol and lactate) increases cytotoxicity despite maintenance of cellular ATP content (31). Both of these effects are important because increases in the NADH-to-NAD ratio and depletion of GSH have been implicated in decreases of the Bcl-Xl-to-Bax ratio, release of cytochrome *c*, and signaling of the execution phase of apoptosis (11, 26).

Another major difference between the groups during the experiment was the attenuation of the changes in acid-base measurements in the pyruvate group. There are two potential causes for this effect. First, pyruvate metabolism is associated with a natural consumption of hydrogen ions. Second, the administration of sodium pyruvate causes marked decrease in serum chloride (21). Sodium pyruvate administration increase sodium from ≈140 to 165 meg/dl and causes a decrease in Cl from ≈100 to 90 meq/dl. In contrast, the hypertonic NaCl solution increased both the serum Na from ≈140 to 170 meg/dl and the Cl from ≈100 to 125 meq/dl. While the impact of the hyperchloremia due to the 10% hypertonic saline on acid-base parameters appears to be negligible compared with the normal saline control (Table 2), the impact of the hypochloremia on the alkalinization effect in the pyruvate group is unknown. However, the impact of these changes on apoptosis in vivo is unclear. In vitro studies of the relationship between acidosis and apoptosis provide conflicting results (9, 10, 37). Furthermore, the effects of other methods of systemic alkalinization were not evaluated because the use of bicarbonate or Carbicarb has not been shown to be beneficial in improving outcome during hemorrhagic shock (2, 3). Even so, the administration of other metabolizable alkalinizing agents such as sodium acetate or sodium β-hydroxybutyrate may help delineate the impact of the pyruvate-induced serum chloride changes on acid-base parameters and indicators of cellular compromise.

While the exact mechanism for pyruvate favorably altering early indicators of apoptosis cannot be determined from the current experiments, changes in the redox state are known to play a major role in the initiation phase of apoptosis. In addition to the known beneficial changes in the MPTP by pyruvate, the redox sensitive antiapoptotic protein Bcl-Xl also blocks the release of cytochrome *c*. Decreasing the release of cytochrome *c* is important because cytochrome *c* irreversibly commits the cell to death by activating caspase 3 and the degradation phase of apoptosis. Activation of caspase 3 has been linked to the proteolytic cleavage of cellular substrates including PARP, a strong indicator of apoptosis (6, 13, 35). Although some studies have shown that Bcl2 and Bcl-Xl are equally effective in preventing apoptosis, others have suggested that overexpression of Bcl-Xl is more important in the protection of apoptosis induced by ischemia-reperfusion (8, 46). In accordance with these observations, an increase in Bcl-Xl protein in the pyruvate-treated group suggests that apoptosis in liver cells caused by hemorrhagic shock can be prevented by the use of pyruvate.

In this study, favorable changes in the Bcl-Xl-to-Bax ratio and the prevention of release of cytochrome *c* from mitochondria were apparent in pyruvate-treated animals. Our data further substantiate that pyruvate can prevent apoptosis by inhibiting the cleavage of caspase 3 because the OD of the cleaved 21-kDa protein was significantly less in the pyruvate-treated group than the 0.9% and 10% NaCl animals. Subsequently, PARP cleavage was reduced when compared with the 0.9% and 10% NaCl groups of animals.

In recent years, evidence has accumulated that increased production of free radicals and apoptosis is a main factor in liver dysfunction after hemorrhagic shock (33). Hepatic apoptosis has been demonstrated in animals subjected to ischemia-reperfusion damage and has been shown to impair hepatocyte function (33). The significance of apoptosis-mediated cell death in the generation of MOF during hemorrhagic shock has been closely examined in a murine model of hemorrhage and resuscitation. In comparing mice genetically deficient in PARP with wild-type mice, the results indicate that PARP activation was associated with hepatic dysfunction and decreases survival. However, this damaging sequence of events was not seen in PARP-deficient mice with hemorrhagic shock (24). In addition, other studies of rats undergoing hemorrhagic shock and resuscitation have shown that the prevention of PARP activation decreases hepatic damage and dysfunction (28, 45). In our study, PARP fragmentation was significantly prevented by pyruvate administration compared with the 0.9% and 10% NaCl groups of swine. This decrease in PARP fragmentation suggests that pyruvate therapy may also help to ameliorate or even prevent the hepatocellular dysfunction that occurs after hemorrhagic shock and resuscitation.

In summary, we demonstrated that pyruvate delays cardiovascular decompensation and decreases early indicators of hepatic apoptosis in this swine model of severe isobaric hemorrhagic shock. Furthermore, this study suggests that the protection offered by exogenous pyruvate could be related to alteration in the cytosolic redox state, acid-base status, or improvement in antioxidant reserves.

This work was supported in part by the Office of Naval Research and the Office of Research and Development, Medical Research Service, Department of Veterans Affairs, and in part by the Division of Surgery, Walter Reed Army Institute of Research.

The opinions or assertions contained herein are the private views of the authors and are not to be construed as reflecting the views of

the Department of the Army, the Department of Defense, or the Department of Veterans Affairs.

REFERENCES

1. **Andreyev A and Fiskum G.** Calcium induced release of mitochondrial cytochrome *c* by different mechanisms selective for brain versus liver. *Cell Death Differ* 6: 825–832, 1999.
2. **Beech JS, Nolan KM, Iles RA, Cohen RD, Williams SC, and Evans SJ.** The effects of sodium bicarbonate and a mixture of sodium bicarbonate and carbonate ("Carbicarb") on skeletal muscle pH and hemodynamic status in rats with hypovolemic shock. *Metabolism* 43: 518–522, 1994.
3. **Benjamin E, Oropello JM, Abalos AM, Hannon EM, Wang JK, Fischer E, and Iberti TJ.** Effects of acid-base correction on hemodynamics, oxygen dynamics, and resuscitability in severe canine hemorrhagic shock. *Crit Care Med* 22: 1616–1623, 1994.
4. **Bernocchi P, Ceconi C, Cargnoni A, Pedersini P, Curello S, and Ferrari R.** Extraction and assay of creatine phosphate, purine, and pyridine nucleotides in cardiac tissue by reversed-phase high-performance liquid chromatography. *Anal Biochem* 222: 374–379, 1994.
5. **Borle AB and Stanko RT.** Pyruvate reduces anoxic injury and free radical formation in perfused rat hepatocytes. *Am J Physiol Gastrointest Liver Physiol* 270: G535–G540, 1996.
6. **Boulares AH, Zoltoski AJ, Contreras FJ, Yakovlev AG, Yoshihara K, and Smulson ME.** Regulation of DNAS1L3 endonuclease activity by poly(ADP-ribosyl)ation during etoposide-induced apoptosis. Role of poly(ADP-ribose) polymerase-1 cleavage in endonuclease activation. *J Biol Chem* 277: 372–378, 2002.
7. **Chang CG, Van Way CW, Dhar A, Helling T, and Hahn Y.** The use of insulin and glucose during resuscitation from hemorrhagic shock increases hepatic ATP. *J Surg Res* 92: 171–176, 2000.
8. **Clem RJ, Cheng EH, Karp CL, Kirsch DG, Ueno K, Takahashi A, Kastan MB, Griffin DE, Earnshaw WC, Veliuona MA, and Hardwick JM.** Modulation of cell death by Bcl-XL through caspase interaction. *Proc Natl Acad Sci USA* 95: 554–559, 1998.
9. **D'Arcangelo D, Facchiano F, Barlucchi LM, Melillo G, Illi B, Testolin L, Gaetano C, and Capogrossi MC.** Acidosis inhibits endothelial cell apoptosis and function and induces basic fibroblast growth factor and vascular endothelial growth factor expression. *Circ Res* 86: 312–318, 2000.
10. **Ding D, Moskowitz SI, Li R, Lee SB, Esteban M, Tomaselli K, Chan J, and Bergold PJ.** Acidosis induces necrosis and apoptosis of cultured hippocampal neurons. *Exp Neurol* 162: 1–12, 2000.
11. **Domenicotti C, Paola D, Vitali A, Nitti M, d'Abramo C, Cottalasso D, Maloberti G, Biasi F, Poli G, Chiarpotto E, Marinari UM, and Pronzato MA.** Glutathione depletion induces apoptosis of rat hepatocytes through activation of protein kinase C novel isoforms and dependent increase in AP-1 nuclear binding. *Free Radic Biol Med* 29: 1280–1290, 2000.
12. **Fernandes RS and Cotter TG.** Apoptosis or necrosis: intracellular levels of glutathione influence mode of cell death. *Biochem Pharmacol* 48: 675–681, 1994.
13. **Galvez A, Morales MP, Eltit JM, Ocaranza P, Carrasco L, Campos X, Sapag-Hagar M, Diaz-Araya G, and Lavandero S.** A rapid and strong apoptotic process is triggered by hyperosmotic stress in cultured rat cardiac myocytes. *Cell Tissue Res* 304: 279–285, 2001.
14. **Halestrap AP, Doran E, Gillespie JP, and O'Toole A.** Mitochondria and cell death. *Biochem Soc Trans* 28: 170–177, 2000.
15. **Halestrap AP, Kerr PM, Javadov S, and Woodfield KY.** Elucidating the molecular mechanism of the permeability transition pore and its role in reperfusion injury of the heart. *Biochim Biophys Acta* 1366: 79–94, 1998.
16. **Heckbert SR, Vedder NB, Hoffman W, Winn RK, Hudson LD, Jurkovich GJ, Copass MK, Harlan JM, Rice CL, and Maier RV.** Outcome after hemorrhagic shock in trauma patients. *J Trauma* 45: 545–549, 1998.
17. **Hirsch T, Susin SA, Marzo I, Marchetti P, Zamzami N, and Kroemer G.** Mitochondrial permeability transition in apoptosis and necrosis. *Cell Biol Toxicol* 14: 141–145, 1998.
18. **Kashiwagi A, Nishio Y, Asahina T, Ikebuchi M, Harada N, Tanaka Y, Takahara N, Taki H, Obata T, Hidaka H, Saeki Y, and Kikkawa R.** Pyruvate improves deleterious effects of high glucose on activation of pentose phosphate pathway and glutathione redox cycle in endothelial cells. *Diabetes* 46: 2088–2095, 1997.
19. **Kerr PM, Suleiman MS, and Halestrap AP.** Reversal of permeability transition during recovery of hearts from ischemia and its enhancement by pyruvate. *Am J Physiol Heart Circ Physiol* 276: H496–H502, 1999.
20. **Khan S and O'Brien P.** Rapid and specific efflux of glutathione before hepatocyte injury induced by hypoxia. *Biochem Biophys Res Commun* 238: 320–322, 1997.
21. **Kobelt F, Schreck U, and Henrich HA.** Involvement of liver in the decompensation of hemorrhagic shock. *Shock* 2: 281–288, 1994.
22. **Kroemer G, Dallaporta B, and Resche-Rigon M.** The mitochondrial death/life regulator in apoptosis and necrosis. *Annu Rev Physiol* 60: 619–642, 1998.
23. **Leist M, Gantner F, Bohlinger I, Tiegs G, Germann PG, and Wendel A.** Tumor necrosis factor-induced hepatocyte apoptosis precedes liver failure in experimental murine shock models. *Am J Pathol* 146: 1220–1234, 1995.
24. **Liaudet L, Soriano FG, Szabo E, Virag L, Mabley JG, Salzman AL, and Szabo C.** Protection against hemorrhagic shock in mice genetically deficient in poly(ADP-ribose)polymerase. *Proc Natl Acad Sci USA* 97: 10203–10208, 2000.
25. **Marchetti P, Castedo M, Susin SA, Zamzami N, Hirsch T, Macho A, Haeffner A, Hirsch F, Geuskens M, and Kroemer G.** Mitochondrial permeability transition is a central coordinating event of apoptosis. *J Exp Med* 184: 1155–1160, 1996.
26. **Marchetti P, Decaudin D, Macho A, Zamzami N, Hirsch T, Susin SA, and Kroemer G.** Redox regulation of apoptosis: impact of thiol oxidation status on mitochondrial function. *Eur J Immunol* 27: 289–296, 1997.
27. **Maulik N, Sasaki H, Addya S, and Das DK.** Regulation of cardiomyocyte apoptosis by redox-sensitive transcription factors. *FEBS Lett* 485: 7–12, 2000.
28. **McDonald MC, Mota-Filipe H, Wright JA, Abdelrahman M, Threadgill MD, Thompson AS, and Thiemermann C.** Effects of 5-aminoisoquinolinone, a water-soluble, potent inhibitor of the activity of poly (ADP-ribose) polymerase on the organ injury and dysfunction caused by haemorrhagic shock. *Br J Pharmacol* 130: 843–850, 2000.
29. **Mongan PD, Capacchione J, Fontana JL, West S, and Bunger R.** Pyruvate improves cerebral metabolism during hemorrhagic shock. *Am J Physiol Heart Circ Physiol* 281: H854–H864, 2001.
30. **Mongan PD, Fontana JL, Chen R, and Bunger R.** Intravenous pyruvate prolongs survival during hemorrhagic shock in swine. *Am J Physiol Heart Circ Physiol* 277: H2253–H2263, 1999.
31. **Niknahad H, Khan S, and O'Brien PJ.** Hepatocyte injury resulting from the inhibition of mitochondrial respiration at low oxygen concentrations involves reductive stress and oxygen activation. *Chem Biol Interact* 98: 27–44, 1995.
32. **Remmers DE, Wang P, Cioffi WG, Bland KI, and Chaudry IH.** Chronic resuscitation after trauma-hemorrhage and acute fluid replacement improves hepatocellular function and cardiac output. *Ann Surg* 227: 112–119, 1998.
33. **Sasaki H, Matsuno T, Nakagawa K, Matsuoka J, and Tanaka N.** Superoxide induces hepatocyte apoptosis during the early phase of reperfusion after murine liver ischemia. *Transplant Proc* 30: 2958–2959, 1998.
34. **Schafer FQ and Buettner GR.** Redox environment of the cell as viewed through the redox state of the glutathione disulfide/glutathione couple. *Free Radic Biol Med* 30: 1191–1212, 2001.
35. **Soldani C, Lazze MC, Bottone MG, Tognon G, Biggiogera M, Pellicciari CE, and Scovassi AI.** Poly(ADP-ribose) polymerase cleavage during apoptosis: when and where? *Exp Cell Res* 269: 193–201, 2001.
36. **Tejero-Taldo MI, Caffrey JL, Sun J, and Mallet RT.** Antioxidant properties of pyruvate mediate its potentiation of beta-

adrenergic inotropism in stunned myocardium. *J Mol Cell Cardiol* 31: 1863–1872, 1999.
37. **Thangaraju M, Sharma K, Leber B, Andrews DW, Shen SH, and Srikant CB.** Regulation of acidification and apoptosis by SHP-1 and Bcl-2. *J Biol Chem* 274: 29549–29557, 1999.
38. **Van Way CW, Dhar A, Reddy R, Evans L, Wogahn B, and Helling TS.** Changes in adenine nucleotides during hemorrhagic shock and reperfusion. *J Surg Res* 66: 159–166, 1996.
39. **Vieira HL, Haouzi D, El Hamel C, Jacotot E, Belzacq AS, Brenner C, and Kroemer G.** Permeabilization of the mitochondrial inner membrane during apoptosis: impact of the adenine nucleotide translocator. *Cell Death Differ* 7: 1146–1154, 2000.
40. **Wang P, Ba Z, Dean R, and Chaudry I.** ATP-$MgCl_2$ restores the depressed hepatocellular function and hepatic blood flow following hemorrhage and resuscitation. *J Surg Res* 50: 368–374, 1991.
41. **Wang P, Ba ZF, Morrison MH, Ayala A, and Chaudry IH.** Mechanism of the beneficial effects of pentoxifylline on hepatocellular function after trauma hemorrhage and resuscitation. *Surgery* 112: 451–458, 1992.
42. **Wang P, Hauptman JG, and Chaudry IH.** Hemorrhage produces depression in microvascular blood flow which persists despite fluid resuscitation. *Circ Shock* 32: 307–318, 1990.
43. **Wang P, Hauptman JG, and Chaudry IH.** Hepatocellular dysfunction occurs early after hemorrhage and persists despite fluid resuscitation. *J Surg Res* 48: 464–470, 1990.
44. **Wang TG, Gotoh Y, Jennings MH, Rhoads CA, and Aw TY.** Lipid hydroperoxide-induced apoptosis in human colonic CaCo-2 cells is associated with an early loss of cellular redox balance. *FASEB J* 14: 1567–1576, 2000.
45. **Watts JA, Grattan RM, Whitlow BS, and Kline JA.** Activation of poly(ADP-ribose) polymerase in severe hemorrhagic shock and resuscitation. *Am J Physiol Gastrointest Liver Physiol* 281: G498–G506, 2001.
46. **Yang Z, Zingarelli B, and Szabo C.** Effect of genetic disruption of poly (ADP-ribose) synthetase on delayed production of inflammatory mediators and delayed necrosis during myocardial ischemia-reperfusion injury. *Shock* 13: 60–66, 2000.